A Study of Fracture in High Purity 7075 Aluminum Alloys

JOSEPH S. SANTNER

Ten different alloys based on the 7075 composition were used to study the effect of purity level, dispersoid type, and heat treatment on fracture toughness. Five purity levels ranging from 0.03 to 0.30 wt pct Fe + Si and two dispersoid types were investigated. Each alloy was given two heat treatments: the standard T651 heat treatment or a special thermomechanical treatment (TMT). Fracture toughness was measured using notched round tensile specimens taken from both the longitudinal and long-transverse directions. The notched round tensile test was modified to give the "plastic energy per unit area". This fracture toughness parameter gave the same ranking for corresponding alloy/heat treatment combinations as the total energy per unit area measured on precracked Charpy specimens. The fracture toughness ranking for the ten alloys was the same in the longitudinal and long-transverse directions. This suggests the elongated distribution of constituent particles in the rolling direction does not change the failure mechanism. Fractographic evidence showed a bimodal distribution of ductile dimple size in all ten alloys. The number of large ductile dimples decreased with increasing purity level while the number of small ductile dimples increased. This is interpreted to mean that the smaller dispersoid and hardening particles become increasingly important in controlling the fracture toughness as the large intermetallic particles are eliminated by increasing the purity of these aluminum alloys. Since thermomechanical processing controls the amount and type of these smaller particles, it is a useful means for increasing fracture toughness in high purity aluminum alloys.

I. INTRODUCTION

ALUMINUM alloys used by the aerospace industry must simultaneously have high tensile strength and fracture toughness with good corrosion and fatigue resistance if aerodynamically efficient structures are to operate economically in service. Strength, toughness, corrosion and fatigue resistance are influenced by both the alloy chosen and the processing sequence used to fabricate the component, be it cast, forged, extruded or machined from wrought plate/sheet. Each of these material processes produces different grain textures and precipitate dispersion within the grains. A systematic study of the relationship between the mechanical properties and the precipitates commonly found in wrought aluminum plate was undertaken.[1-3] This work discusses the relation between fracture toughness and the various precipitates.

Generally, the precipitates are classified into three types: constituent particles, dispersoid particles, and hardening particles. They are grouped into one of these three categories according to the order in which they appear during the processing sequence. The constituent particles precipitate from the molten solution during solidification of the ingot. They are thermodynamically the most stable. From the practical point of view, subsequent processing will have little effect on changing the size of these particles, though extensive mechanical working can change their distribution somewhat. These iron and silicon rich particles have incoherent interfaces with the matrix and range in size from 5 to 30 μm. The dispersoid particles precipitate from solid solution during the homogenizing solution treatment of the ingot. These particles are, for example, chromium or zirconium-rich, ranging in size from 0.03 to 0.3 μm. The hardening particles are thermodynamically the least stable and they can precipitate from the solid solution at room temperature. They range in size from 50Å (5 nm) to 500Å (50 nm), having either coherent or incoherent interfaces. The high strengths exhibited by the 7000 series alloys for example, are produced by zinc-rich precipitates upon warm aging.

In so far as the effect of constituent particles on toughness is concerned, previous work[4] has demonstrated that high purity 7000 series aluminum alloys have a dramatically improved strength *vs* toughness trend over those of commercially pure 7000 series aluminum alloys. Both the amount (volume fraction) and size of the constituent particles determine the purity of an alloy. For example, by specifying higher purity alloys in forgings such as 7175 over 7075, cost penalties are incurred. The level of purity above which fracture toughness cannot be improved by this technical approach has economic consequences.

For the dispersoid particles, studies have shown[5] replacing the normal chromium dispersoid with zirconium in 7075 has improved fracture toughness with no loss of strength. The aluminum alloy 7050 was developed based on the observation that zirconium improves toughness. However, the causes for this improvement are not completely understood.

The effect of the hardening particles on fracture toughness has received less attention. This may be due to the general empirical observation that by increasing the strength of an alloy through heat treatment, its fracture toughness is simultaneously de-

JOSEPH S. SANTNER is Project Engineer, Metals and Ceramics Division, Air Force Materials Laboratory, Wright-Patterson Air Force Base, OH 45433.

Manuscript submitted March 24, 1977.

ISSN 0360-2133/78/0612-0769$00.75/0

Table I. Compositions of Experimental and Commercial Alloys

Composition	7475	A	B	C	D	E
Zn	5.2 to 6.2	5.89	5.91	5.93	5.93	5.94
Mg	1.9 to 2.6	2.19	2.42	2.39	2.35	2.36
Cu	1.2 to 1.9	1.50	1.58	1.60	1.64	1.63
Cr	0.18 to 0.25	0.21	0.22	0.21	0.21	0.21
Fe	0.12	0.02	0.05	0.08	0.12	0.20
Si	0.10	0.01	0.02	0.04	0.06	0.11
Mn	0.06	<0.01	<0.01	<0.01	<0.01	<0.01
Ti	0.06	0.004	0.005	0.012	0.012	0.009
Others (Total)	0.15	<0.01	<0.01	<0.01	<0.01	<0.01

Composition	7050	Al	Bl	Cl	Dl	El
Zn	5.7 to 6.7	5.73	5.68	5.84	6.02	5.98
Mg	1.9 to 2.6	2.39	2.31	2.31	2.33	2.45
Cu	2.0 to 2.8	1.50	1.51	1.54	1.51	1.52
Zr	0.08 to 0.15	0.12	0.12	0.12	0.12	0.12
Fe	0.15	0.01	0.04	0.08	0.11	0.20
Si	0.12	0.01	0.02	0.04	0.05	0.09
Mn	0.10	0.01	0.01	0.01	0.01	0.01
Ti	0.06	0.004	0.005	0.006	0.005	0.006
Cr	0.04	<0.01	<0.01	<0.01	<0.01	<0.01
Other (Total)	0.10	<0.01	<0.01	<0.01	<0.01	<0.01

creased.[6] However, there have been exceptions to this trend[7] which suggest that each type of precipitate, plus its possible interaction with one another, must be considered. The present study was conducted to better understand the role all three precipitate types play in the fracture of aluminum alloys.

II. EXPERIMENTAL

1. Materials

In order to systematically study the effects of constituent, dispersoid, and hardening particles in wrought aluminum plate, a series of alloys was obtained based on the composition of 7075. To study the effects of constituent particles, five different combined purity levels of iron and silicon were used ranging from 0.03 wt pct to 0.3 wt pct with the ratio of iron to silicon being held constant at two. For identification purposes, they are labeled "A" through "E" with the most pure called "A".

To assess the role of dispersoid particles and their interaction with the iron and silicon, both chromium and zirconium were separately added to each of the five purity level alloys for a total of ten different alloys. A second digit is added (one) to identify the five zirconium-bearing alloys (A1, B1, C1, D1, E1). The compositions of the ten experimental alloys are given in Table I along with the composition of 7475 and 7050. These alloys are included to illustrate several points. The experimental chromium-bearing alloys A through E are compared with 7475 which is the highest purity commercial alloy. The alloy 7175 which is the other high purity version of 7075 is only available as a forging and not as a plate product and it is less pure than 7475. The experimental zirconium-bearing alloys A1 through E1 are compared with 7050 because this is the modern 7000 series alloy which uses zirconium as a dispersoid and has high purity specifications. However, 7050 is quite different from the experimental alloys in that it has a higher zinc and copper content.

Two different heat treatments (T651 and TMP) were used on all ten alloys to study the role of hardening particles. The T651 process involves a 1.5 pct stretch prior to a 24 h age at 250°F (121°C) followed by air cooling. The TMP process used is actually a FTMP according to the nomenclature developed by Waldman, *et al*[8] as it occurs after the final solution treatment. Four hours aging at 250°F (121°C) and a 20 min age at 325°F (163°C) precede a 25 pct reduction by warm rolling at 302°F (150°C) to 0.625 in. (1.59 cm) and a 1.5 pct stretch. Final aging for two hours at 290°F (143°C) was used for two of the ten alloys (B1 and C1) in order to increase their yield strengths to levels approaching the 7075-T651 strength levels. Both the longitudinal and long-transverse average tensile yield strengths are given in Table II for all ten alloys.[1] Previous metallographic work[9] has shown that the wrought product grain structure is anisotropic in the alloys. This is evident from the average tensile yield strength given in Table II.

2. Modified Notched Tensile Test

The notched-yield ratio, the ratio of notched tensile strength to the smooth bar yield strength, was not used to characterize toughness in the present study. Plots of K_{IC} *vs* the notch-yield ratio (N-YR), Ref. 12, show an exponential shape so that for notch-yield ratios greater than 1.3, a small difference in the measured N-YR makes a large difference in the predicted K_{IC}. Since most of the experimental alloys had higher purity levels than 7475, high toughness values were anticipated with a N-YR greater than 1.3. Assuming the microscopic plastic deformation is the physical reason for the increased toughness one concludes that load is, in itself, not a sufficient measure of fracture toughness under these test conditions. For this reason, the notched tensile test was modified to obtain simultaneously both load and deformation information.

Following the proposed ASTM test method for notched tensile tests,[10] 0.5 in. (1.27 cm) diam specimens were machined to the prescribed geometry. Specimens in the longitudinal and long-transverse directions were tested because of the elongated grain structure which affected the yield strength. A 50 KIP capacity Instron tensile test machine was used with a

Table II. Average Tensile Yield Strength* of the Ten Experimental Alloys in the Longitudinal and Long-Transverse Directions

	Longitudinal Direction		Long-Transverse Direction	
	T651	TMP	T651	TMP
A	73.0 (504)	62.7 (433)	63.6 (439)	56.3 (388)
B	73.8 (509)	66.0 (455)	61.6 (425)	57.9 (400)
C	75.1 (518)	62.1 (428)	64.7 (446)	55.0 (380)
D	72.6 (501)	68.3 (471)	62.0 (428)	57.1 (394)
E	68.8 (475)	66.9 (462)	60.5 (417)	54.6 (377)
Al	77.4 (534)	66.5 (459)	62.6 (432)	56.3 (388)
Bl	74.2 (512)	62.4 (431)	65.4 (451)	58.7 (402)
Cl	76.1 (525)	63.8 (440)	61.6 (425)	59.7 (412)
Dl	79.7 (550)	64.9 (448)	66.2 (457)	57.4 (396)
El	79.5 (549)	67.9 (469)	64.6 (446)	56.5 (390)

*The 0.2 pct offset yield strength is given in units of KSI (MPa).

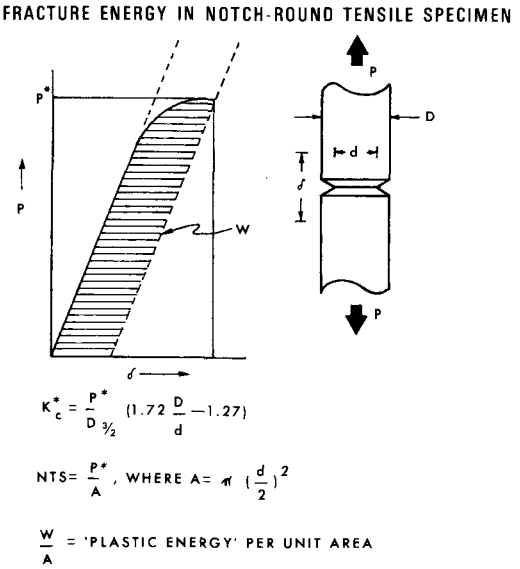

Fig. 1—Schematic of typical load *vs* extensometer displacement output from a notched round tensile test.

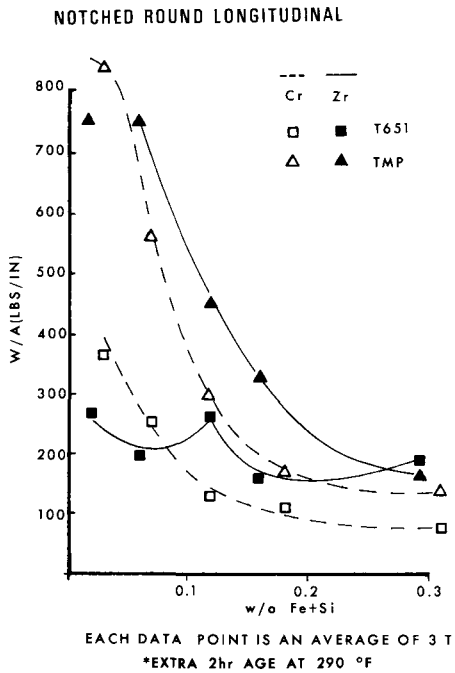

Fig. 2—W/A *vs* wt pct Fe + Si for notched round longitudinal specimens of 7X75 alloys with T651 and TMP heat treatments.

universal joint threaded onto each end of the specimen. With this configuration the measured percent bending stress for a 0.5 in. (1.27 cm) diam steel specimen was consistently below 10 pct at 30 KSI (207 Mpa) stress level. In addition to measuring the load at failure, the specimen elongation was monitored by means of a $\frac{1}{2}$ in. (1.27 cm) clip-on extensometer. Since the area of the notched cross section is half of the unnotched portion, with a K_t of 11, the measured deformation is approximately that experienced by the material in the notch.[11] The load *vs* displacement output was recorded on an X-Y plotter. A schematic drawing of a typical test record is given in Fig. 1. The shaded area under the load *vs* displacement curve is used to calculate the "plastic energy per unit area", W/A.

The rationale for using this test procedure to measure toughness is based on the idea that ductile fracture in its most general form is a two step process as summarized by Thompson and Weihrauch.[13] The first step involves the nucleation of voids at the "macroinclusion", *i.e.*, inclusions greater than 1 μm in diam. The second step is the coalescence of the microcracks by the formation of shear bands or void sheets between the "macroinclusions". If a material fails by the nucleation of voids at the "macroinclusions" before the shearing process becomes fully developed, its elongation will be significantly less than a material where void sheets must be developed under Mode II crack opening between "macroinclusions".

III. RESULTS

1. Notched Tensile Tests

The plastic energy absorbed per unit area, W/A, is plotted as a function of the combined iron and silicon content in Figs. 2 and 3 for the longitudinal and long-transverse specimens, respectively. Each data point is the average of three test results. One curve is drawn through each combination of dispersoid type and heat treatment. The four curves in each figure show the same trends. Both heat treatments for the chromium-bearing alloys (dashed lines) increase their absorbed energy with increasing purity. This is not the case for the zirconium-bearing alloys (solid lines). Increasing their purity beyond a certain critical purity level apparently decreases the fracture toughness. This purity level is defined as the transition purity level. Above the critical transition purity levels, the zirconium alloys have a larger fracture toughness than the chromium alloys given the same heat treatment. Below the critical transition purity levels, the fracture toughness advantage found in the

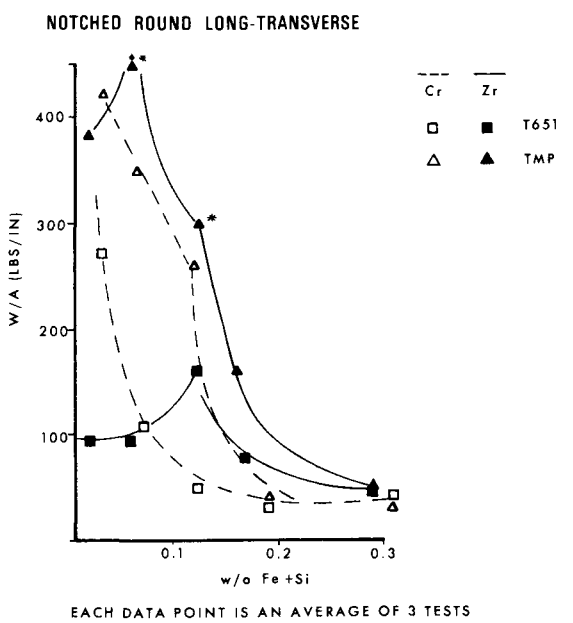

Fig. 3—W/A *vs* wt pct Fe + Si for notched round long-transverse specimens of 7X75 alloy with T651 and TMP heat treatment.

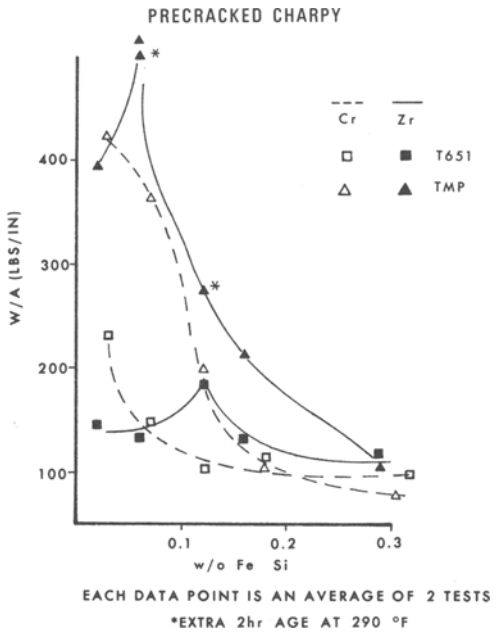

Fig. 4—W/A *vs* wt pct Fe + Si for precracked Charpy T-L specimens of 7X75 alloys with the T651 and TMP heat treatments from Ref. 3.

zirconium alloys is lost. The transition purity level is a function of the heat treatment for the zirconium-bearing alloys. For the T651 heat treatment the transition occurs at approximately 0.12 wt pct Fe + Si while the transition occurs at approximately 0.06 wt pct Fe + Si for the TMP heat treatment.

An analysis of variance highlighted a fact that can be overlooked in Figs. 2, 3 and 4. Heat treatment, purity level, and the interaction between heat treatment and purity levels are, in that order, the three most important factors controlling the absorbed energy by these materials. If the data in Fig. 3 is replotted by combining the open and closed symbols for each heat treatment beyond the purity level of 0.22 wt pct

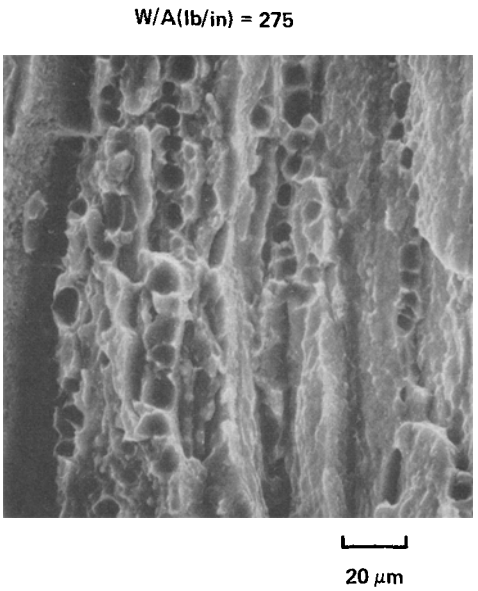

(a)

Fig. 5—Typical fracture areas of chromium-bearing alloys in the T651 condition, (*a*) 0.03 wt pct Fe + Si, (*b*) 0.12 wt pct Fe + Si, (*c*) 0.31 wt pct Fe + Si. Magnification 500 times.

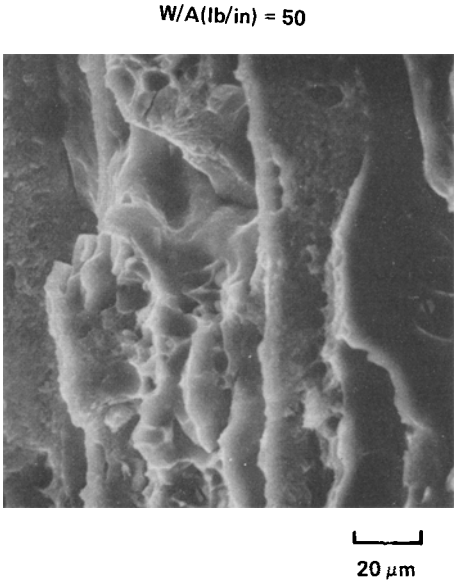

(b)

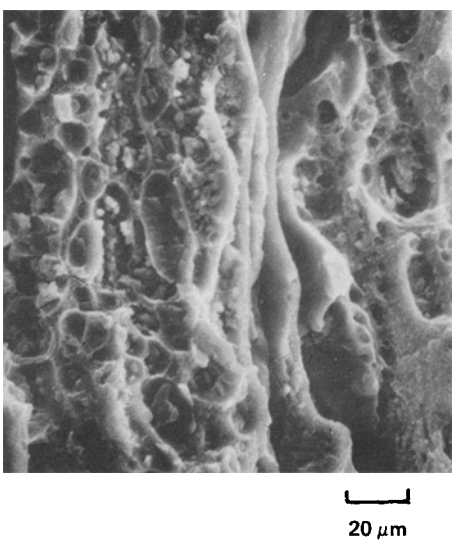

(c)

Fe + Si, the TMP specimens given greater W/A than the T651 specimens.

Since both heat treatments show increasing toughness with increasing purity level, the importance of purity is evident. However, the TMP specimens show a greater increase in W/A than the T651 specimens at any purity level, implying an interaction between purity level and heat treatment. However, these results must be tempered with the fact that all the experimental alloys have purity greater than or equal to commercial 7475 aluminum, the high purity version of 7075.

2. Fractography

Since the corresponding four curves for longitudinally oriented specimens (Fig. 2) display the same trends as material tested in the long-transverse direction (Fig. 3), fractographic studies are limited to the latter. Using notched-round specimens fractured in the transverse plane for these studies has two ad-

vantages. First, these specimens failed macroscopically in a single mode of crack opening (Mode I) rather than the more complex mode found in three point bending. In addition, the interaction between the purity level (constituent particles of Fe and Si) and the dispersoid particles (Cr, Zr) should be more obvious in the transverse plane where elongated stringers of constituent particles would normally dominate the micromechanism of failure.

Figure 5 shows the typical fracture surfaces for the chromium-bearing alloys in the T651 condition. The absorbed energy of these specimens is represented by open squares in Figs. 2 and 3. It is clear that a large number of 2 to 4 μm size second phase particles is nearly homogeneously distributed throughout the fracture surface of the least pure alloys (Figs. 5(*c*)). However, there are discrete patches of the fracture surface which are either smooth or coarse in texture. The intermediate purity alloy (Fig. 5(*b*)) has a smaller fraction of regions containing the 2 to 4 μm size particles and contains more surface with either the smooth or coarse textured areas noted in the least pure alloy. The most pure alloy (Fig. 5(*a*)) has an inhomogeneous distribution of regions containing the 2 to 4 μm size particles. These regions are separated by areas of the coarse texture with no smooth areas as found in the other two alloys. In all three alloys, the coarse textured areas separating the regions containing the 2 to 4 μm size particles are elongated parallel to the plate surface. In addition, 1000 times magnification fractographs of the coarse textured areas show approximately 1.0 μm sized ductile dimples not distinguishable in Fig. 5.

Figure 6 shows the typical fracture surfaces for the zirconium-bearing alloys in the T651 condition. The absorbed energy of these specimens is represented by closed squares in Figs. 2 and 3. Like the chromium-bearing alloys in Fig. 5, the fraction of regions containing the 2 to 4 μm sized particles increases with increasing iron and silicon content. These regions

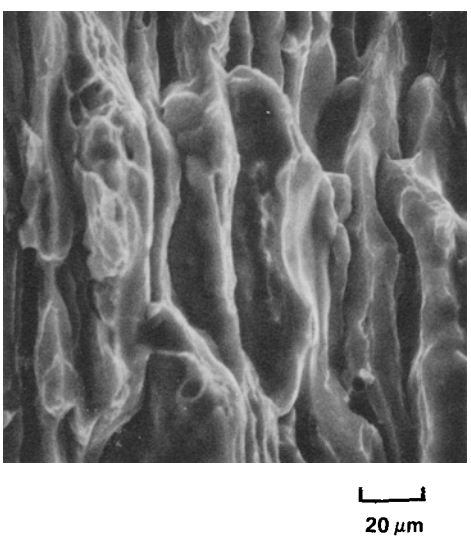

(*a*)

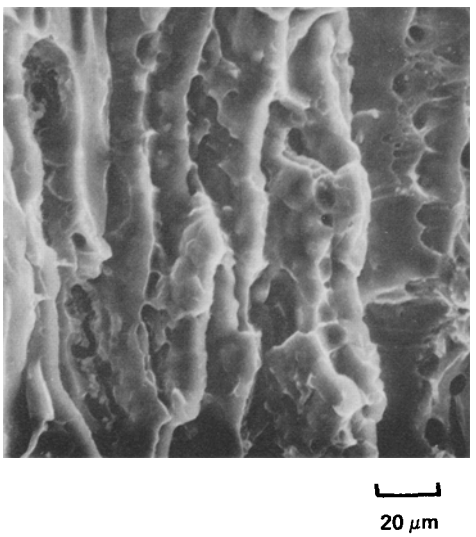

(*b*)

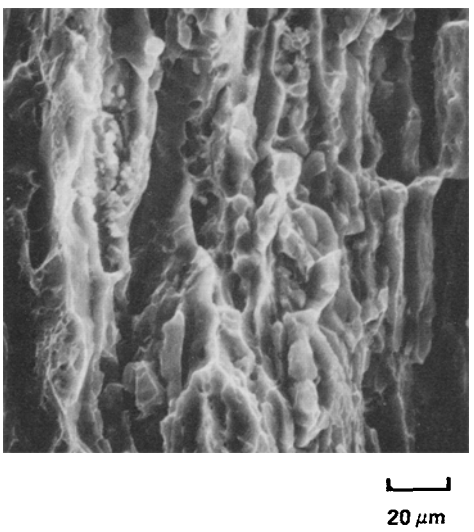

(*c*)

Fig. 6—Typical fracture areas of zirconium bearing alloys in the T651 condition, (*a*) 0.02 wt pct Fe + Si, (*b*) 0.12 wt pct Fe + Si, (*c*) 0.29 wt pct Fe + Si. Magnification 500 times.

are also elongated parallel to the plate surface. Unlike the chromium-bearing alloys in Fig. 5, there are no coarse textured areas containing the finer 1 μm sized ductile dimples at 1000 times magnification.

Figure 7 shows the typical fracture surfaces for the chromium-bearing alloys in the TMP condition. The absorbed energy of these specimens is represented by open triangles in Figs. 2 and 3. Approximately two-thirds of the fracture surface of the 0.18 wt pct Fe + Si alloy (Fig. 7(*b*)) is composed of macrodimples ($\simeq 20 \times 40$ μm) elongated parallel to the plate surface. These are formed from a number of 2 to 4 μm sized particles acting in tandem. The remaining one-third of the fracture surface contains the previously mentioned coarse textured areas. The higher purity alloy (Fig. 7(*a*)) generally does not show the macrodimples formed by a number of 2 to 4 μm particles acting in tandem. Half of its surface contains dimples initiated by the 2 to 4 μm sized particles; the

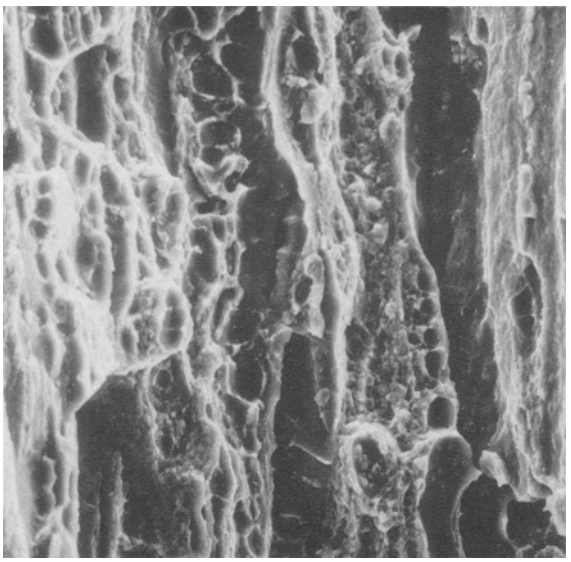

(a)

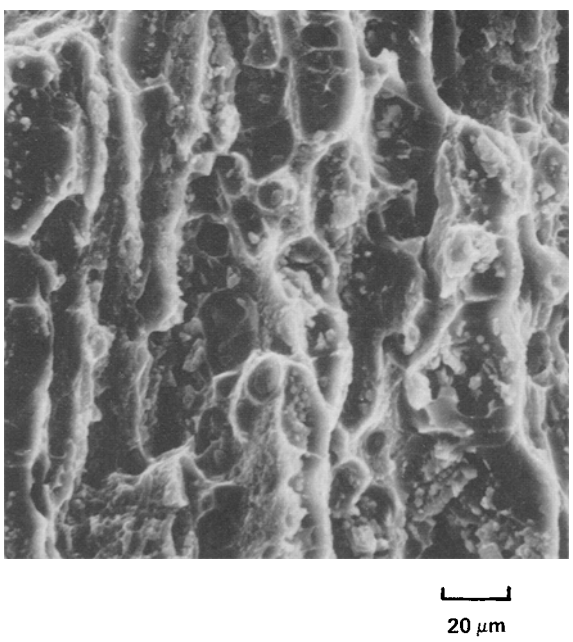

(b)

Fig. 7—Typical fracture areas of chromium bearing alloys in the TMP condition, (*a*) 0.07 wt pct Fe + Si, (*b*) 0.18 wt pct Fe + Si. Magnification 500 times.

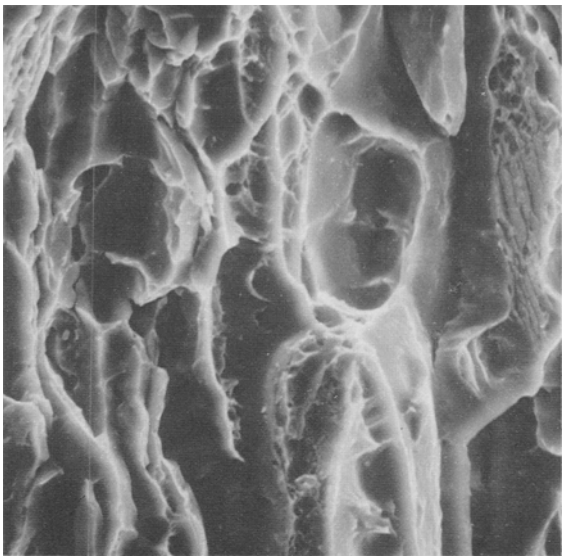

(a)

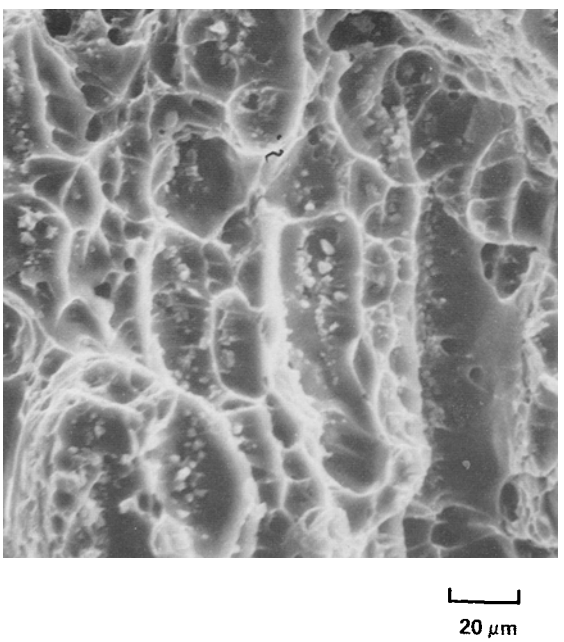

(b)

Fig. 8—Typical fracture areas of zirconium bearing alloys in the TMP condition, (*a*) 0.06 wt pct Fe + Si, (*b*) 0.16 wt pct Fe + Si. Magnification 500 times.

other half has coarse textured areas which consist of approximately 1.0 μm diam ductile dimples (as seen at higher magnifications).

Figure 8 shows the typical fracture surfaces for the zirconium-bearing alloys in the TMP condition. The absorbed energy of these specimens is represented by closed triangles in Figs. 2 and 3. Like the lower purity chromium-bearing alloys, elongated macrodimples (≃20 × 40 μm) initiated by several 2 to 4 μm diam particles acting in tandem are present. However, unlike the chromium-bearing alloys, the coarse textured areas are not present in either the lower or higher purity alloys (0.06 wt pct Fe + Si and 0.16 wt pct Fe + Si, respectively). These areas are replaced by smooth textured areas previously noted for the zirconium-bearing alloys given the T651 heat treatment in Fig. 6. In addition, the elongated macrodimples exist in the higher purity zirconium-bearing alloys, while the chromium-bearing alloys did not show this feature.

IV. DISCUSSION

1. Notched Tensile Tests

Previous work[14] has shown a reasonable correlation between K_{IC}^2/E and W/A for precracked Charpy specimens fractured by slow-bending. Fractographic studies of microdeformation mechanisms is complicated in a three point bend specimen because the material away from the notch, beyond the neutral bending axis, experiences compressive strains during the first part of the test. In addition, shear stresses of the opposite sign operate across the fracture plane. These experimental considerations combined with the fact that precracked slow-bend Charpy results (Fig. 4) indicated decreasing fracture toughness for the highest purity zirconium-bearing alloys,[3] led to the use of notched-round tensile tests. The two test results should give the same results if the observed behavior is due to the material and not the specimen geometry.

A comparison of Figs. 3 and 4 shows the total energy required to fracture precracked Charpy specimens in slow-bend is nearly identical to the "plastic energy" measured from a notched round tensile test. These results are replotted in Fig. 9 and it appears that for small W/A values, the notched round tensile test gives somewhat lower values than the precracked Charpy slow-bend test. The apparent general agreement between the two measures of fracture toughness illustrated in Fig. 9 may be fortuitous and further work is required to answer this question.

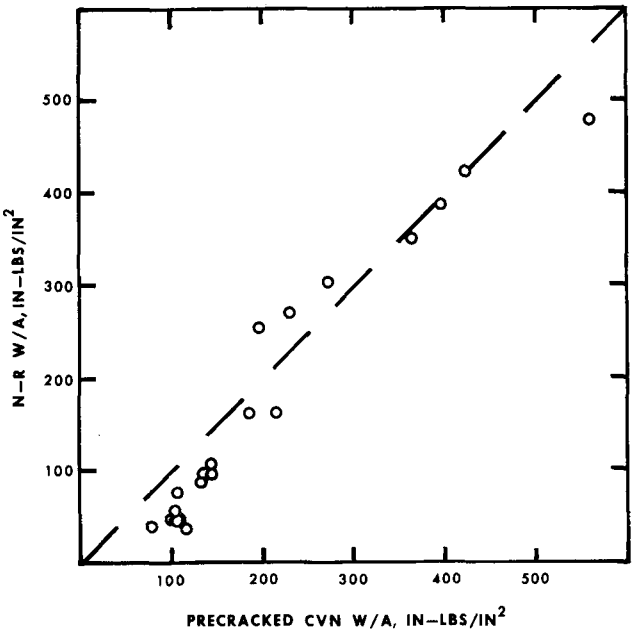

Fig. 9—Comparison of the precracked slow-bend Charpy data to the notched round tensile W/A results.

2. Dispersoid Type and Fracture Toughness

While the scatter for the modified notched round tensile test at this stage of its development appears to be greater than that for the precracked Charpy slow-bend test, the average for three tests shows the same trends (compare Figs. 3 and 4). Namely, the zirconium-bearing alloys appear to have a critical transition level beyond which the fracture toughness is not increased by increasing the purity level. Furthermore, both the longitudinal and the long-transverse data show the same qualitative results but on a different scale for each of the corresponding curves in Figs. 2 and 3.

The decrease of fracture toughness for zirconium-bearing alloys in very high purity 7075 alloys has been reported elsewhere,[15] and is illustrated in Fig. 10. In that study, the 7475 alloys 'B' and 'D' had 0.10 and 0.13 wt pct Fe + Si, respectively, while the 'high purity' 7475 alloys 'C' and 'E' had 0.03 and 0.02 wt pct Fe + Si, respectively. An interesting observation is that the previously defined transition purity level for the T651 temper in the present work is near the same purity level for the 7475 alloys in Fig. 10(*a*) (0.12 wt pct Fe + Si). The self-consistency of the data for the alloys listed in Table I, plus the data from the alloys in an independent study[15] suggest the observed anomaly is real. The earlier work presented data which explains the loss of toughness in terms of the grain size. Unfortunately, no definitive grain size measurements could be made in the present work to test this hypothesis, because of the inhomogeneous grain size of the alloys. This is illustrated in Fig. 11 where an apparent bimodal distribution of grain sizes is qualitatively observed. These fields of view show a large number of equiaxed 5 to 10 μm grains and an equal number of 50 to 100 μm wide by 500 to 1000 μm long grains.

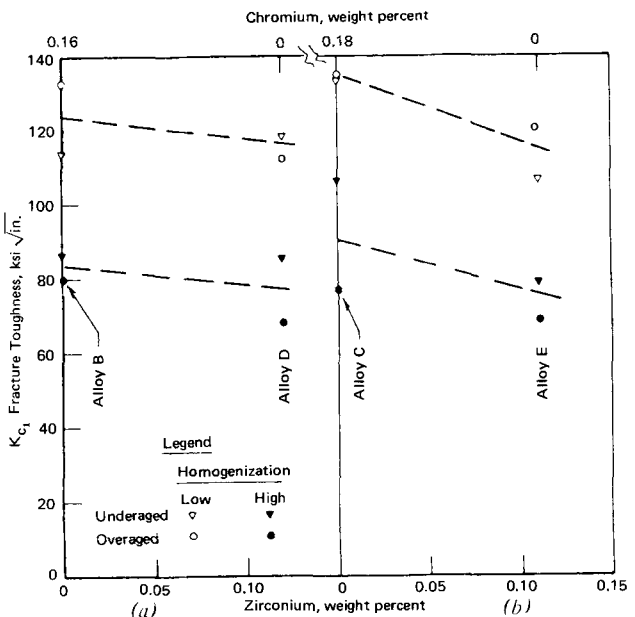

Fig. 10—Effect of fracture toughness due to replacement of chromium by zirconium in 7000-series alloys from Ref. 13. (*a*) 7475: center-cracked panel, (*b*) High-Purity 7475: center cracked panel.

3. Purity Level and Fracture Toughness

The role precipitates play in ductile fracture has been considered from two points of view. One school of thought views ductile fracture to be controlled only by the amount (volume fraction) and distribution (average size) of the large "macroinclusions" (*i.e.* precipitates larger than 1 μm). Using this idea, the following failure criterion was proposed based on metallurgical variables.[16,17]

(a)

(b)

Fig. 11—Bimodal distribution of grain size in zirconium-bearing experimental 7075. A 10 pct phosphoric etch brings out the unrecrystallized grain structure at 100 times: (*a*) E-T651, (*b*) E1-T651.

$$K_{IC} \simeq [2(\tfrac{\pi}{6})^{1/3} \sigma_y E D]^{1/2} f^{-1/6} \quad [1]$$

where f is the volume fraction of a dispersed phase with a diameter D, E is Young's modulus, and σ_y is the yield strength. On the other hand, other investigators[13,18,19] believed that the fracture phenomenon is more complex; smaller particles (sometimes called dispersoids or "microinclusions") form submicron dimples in the process of creating void sheets between the large voids initiated in or around the large constituent particles (sometimes called inclusions or macroinclusions). It has been suggested[19] that to construct a relationship between K_{IC} and metallurgical features, one term should be included for each stage of the fracture process. To test if the first view is consistent with the present results, Eq. [1] was rearranged to give:

$$\frac{K_{IC}^2}{E} \simeq [2(\tfrac{\pi}{6})^{1/3} \sigma_y D] f^{-1/3}. \quad [2]$$

This form was chosen because the notched round W/A gave the same value of energy per unit area as the precracked slow-bend Charpy W/A data. In addition, it has been shown experimentally that the relationship between W/A and K_{IC}^2/E can be represented by the following expression:[14]

$$\frac{K_{IC}^2}{E} = \frac{1}{2(1-\nu^2)} \cdot (\mathrm{W/A}). \quad [3]$$

By combining Eqs. [2] and [3]:

$$(\mathrm{W/A})(1/\sigma_y) = [4(\tfrac{\pi}{6})^{1/3}(1-\nu^2) D] f^{-1/3} \quad [4]$$

is an equation where both the modulus and strength effects on toughness are normalized. Moreover, if the inclusions are solely responsible for the fracture toughness, a log-log plot of $(\mathrm{W/A})(1/\sigma_y)$ *vs* f would give a straight line with a slope of $-1/3$. Figure 12 is a plot of the data from the present study with a least squares linear regression line having a slope of -0.56 and an intercept of 1.28. The intercept of the linear regression is equal to the bracketed expression in Eq. [4] and thus D can be calculated.

This type of analysis leads to several observations. First, despite the experimental scatter, the slope shows a stronger functional dependence of $(\mathrm{W/A})(1/\sigma_y)$ on f than is predicted by Eq. [4]. Second, the calculated diameter (11.31 μm) is far larger than the constituent particles for even the least pure alloys tested in the present work, as was shown in Fig. 11. Finally, one subtle effect is the segregation of the data for the two heat treatments studied. The data for the TMP heat treated alloys lie above the least squares fit line, while nearly all the data for the T651 heat treated alloys fall below the least squares line for volume fractions less than one half percent. A similar segregation is not noted for the series of alloys with different dispersoid types. Furthermore, a least squares fit for the data from each heat treatment gave a better fit than when the data for both heat treatments was analyzed together.

To summarize, despite the differences in yield strength between the two different heat treatments, for a sufficiently small volume fraction of the constituent particles, heat treatment is equally important

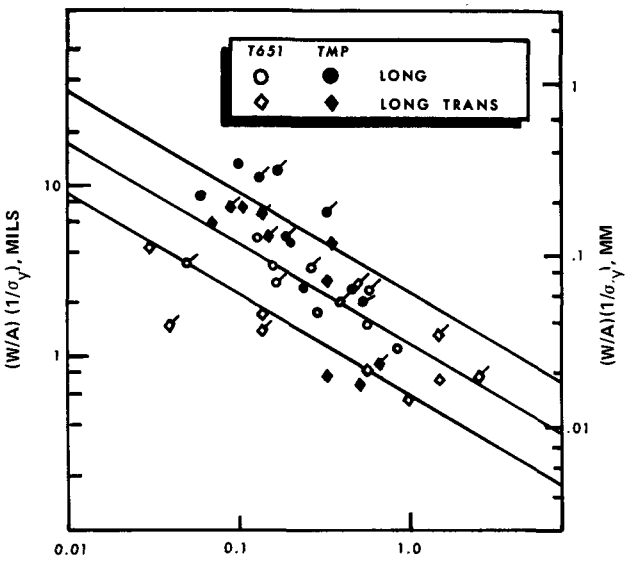

Fig. 12—The influence of volume fraction of large intermetallics on unit fracture energy normalized for yield strength. Data marked by a tick mark are the zirconium-bearing alloys while the remainder of the data is for the chromium-bearing alloys.

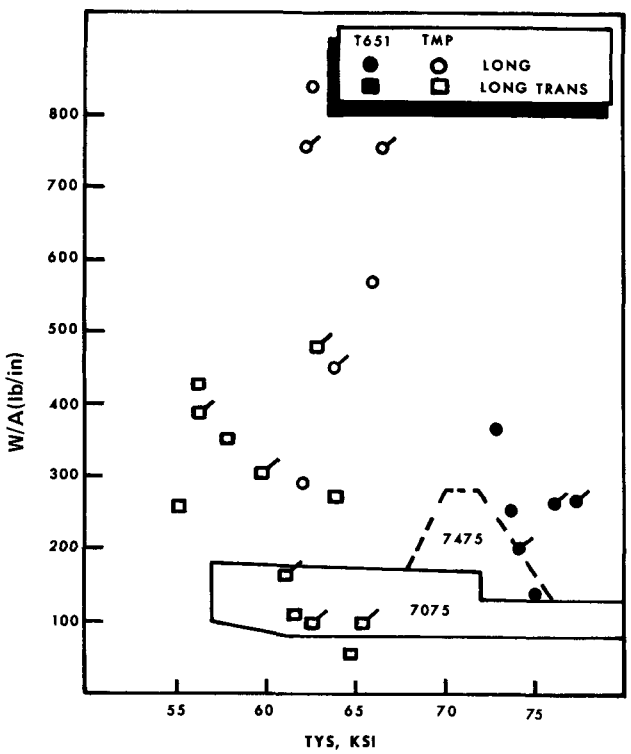

Fig. 13—Effect of heat treatment on W/A for the experimental alloys with ≤0.12 wt pct Fe + Si, compared with T-L and L-T K_{IC} data for commercial 7075 (≃1.2 wt pct Fe + Si) and 7475 (≅0.22 wt pct Fe + Si) plate with various heat treatments with data from Ref. 20.

as the purity level for determining fracture toughness. The sharp rise in W/A below 0.2 wt pct Fe + Si for the TMP heat treated alloys in Figs. 2, 3 and 4 is not due to the experimentally observed effect of increasing toughness with decreasing yield strength. This point is further clarified by Fig. 13 which compares the fracture toughness for commercial heat treatments of 7075 and 7475 to the experimental alloys with less than or equal to 0.12 wt pct Fe + Si. The K_{IC} values were from plate products in the T-L and L-T direction. Equation [3] was used to convert valid K_{IC} values to the equivalent W/A. To avoid confusing the experimental W/A data with the calculated values, the latter are identified by a scatter band. One obvious point is the area marked for 7475 falls below nearly all the experimental alloys given the TMP heat treatment. However, none of the commercial heat treatments of 7475 involved a 25 pct warm rolling at 150°C prior to final aging. This type of processing, as discussed by DiRusso, *et al*[22] and others,[23] produces a dense homogeneous distribution of dislocations. Transmission electron microscope examination of the present alloys yielded pictures nearly identical to those shown by the previous investigators.[23,24]

4. The Null Hypothesis

Even when fracture toughness is normalized for the strength effect, the present evidence suggests that purity level is only one effect controlling this property. The dispersoid and hardening particles in aluminum alloys play an equally important role in determining the fracture toughness. This observation has been made in the past. Experimental evidence presented by Broek[8] is consistent with the two-step mechanism for ductile failure presented by Thompson and Weihrauch.[13] In Broek's study of thirteen commercial aluminum alloys, both small dimples as well as large voids were observed on the fracture surfaces. The previous fractographic evidence makes the same observation. Thus, the required presence of a bimodal distribution of dimple size on a fracture surface is fulfilled.

Broek's study of dimple profiles revealed that the dimples ranging in size from 0.2 to 2.0 μm were relatively shallow holes. Thus, if shear band formation is the second step for ductile fracture mechanism, shallow dimple profiles would be expected. While dimple profiles were not measured in the present study, indirect evidence suggests that shear band formation occurred. In the chromium-bearing alloys, the fractographs clearly showed dimples with these areas described as "being coarse textured" in Figs. 6 and 8. These same coarse textured regions were absent in the zirconium-bearing alloys in Figs. 5 and 7. This does not mean that a finer sized ductile dimple does not exist. Fractographic evidence[20] recently demonstrated that a featureless "rock candy" appearing grain boundary fracture can indeed be a ductile dimple failure at sufficiently high magnification. This work on a high purity binary Al-3.6 wt pct Cu alloy identified a 0.2 μm sphere-like precipitate in the grain boundary responsible for this failure mode.

This hypothesis was tested by performing high magnification TEM replica fractography on the zirconium-bearing alloys. The results of this work is summarized in Fig. 14. The top row refers to material given the T651 heat treatment, while the bottom row represents TMP processed material. The first column refers to the high purity material (Al = 0.02 wt pct Fe + Si) and the last column to the least pure material (El = 0.29 wt pct Fe + Si). In all four cases ductile dimples were

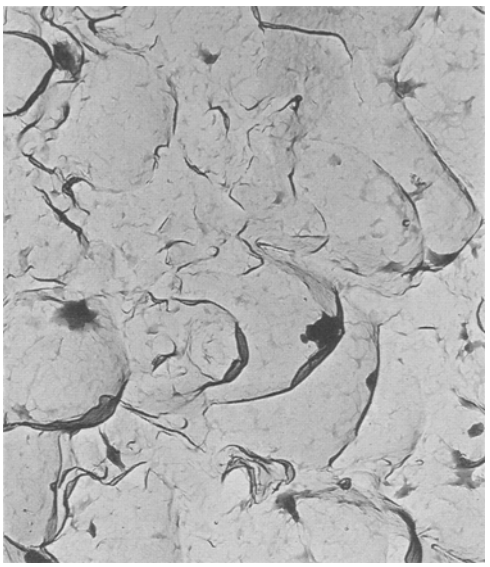

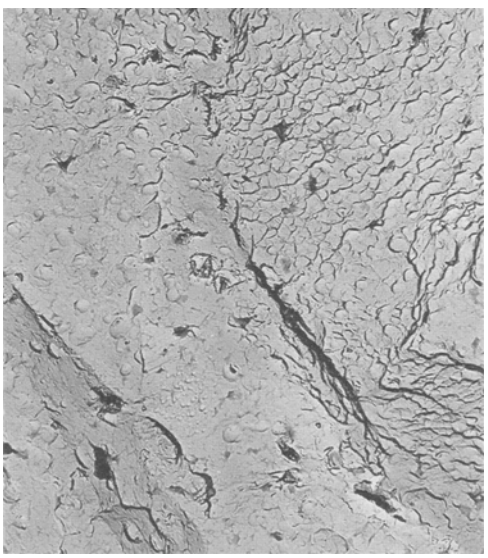

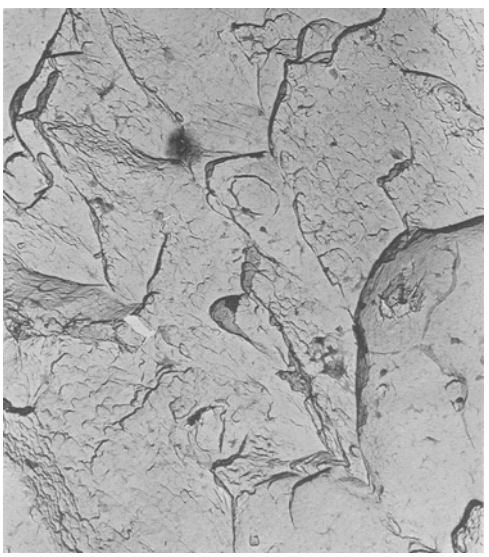

Fig. 14—Replica TEM fractographs of zirconium-bearing alloys showing small ductile dimples formed by the dispersoid and hardening particles: (*a*) Al-T651 (magnification 12,000 times), (*b*) El-T651 (magnification 10,000 times), (*c*) Al-TMP, magnification 7,500 times, (*d*) El-TMP magnification 7,500 times.

observed. For the TMP material the lower magnification permitted observing a bimodal distribution in ductile dimple size. In particular, the A1-TMP fractograph shows 0.25 μm diam ductile dimples. The dimples for the E1-TMP fractograph, while approximately the same size, revealed the presence of more shearing in this particular area. The fractographs for the material with T651 temper were taken at a higher magnification. Both have ductile dimples that were approximately 0.50 μm, about twice as large as that found for the corresponding alloys processed by TMP. Thus, TMP appears to have produced a larger number of the small second phase particle sites than the T651 processed material.

The experimental evidence suggests microvoid coalescence was achieved for both the chromium-bearing and zirconium-bearing aluminum alloys with a total iron and silicon content of less than 0.22 wt pct. The chromium-bearing alloys had clearly visible regions in the shear band containing approximately 1 μm diam dimples, while this was not the case for the zirconium-bearing alloys. The evidence in Fig. 14 suggests that a smaller particle size is responsible for the shear-band formation in the zirconium-bearing alloys. Clearly, more careful quantitative observations of mating fracture surfaces is required before an expression relating K_{IC} to both the constituent particles and dispersoid particles can be developed.

Moreover, the sharp rise in W/A for the TMP heat-treated alloys may involve a more complex mechanism in the formation of void sheets than is the case of alloys without a uniformly dense dislocation substructure.

V. SUMMARY AND CONCLUSIONS

A modified notched round tensile test was used to measure the relative fracture toughness of ten different aluminum alloys based on the 7075 composition. The fracture toughness ranking for these alloys, the plastic energy per unit area, is the same in the longitudinal and long-transverse directions and agrees with the ranking found in precracked Charpy tests.[3] This result suggests that the same micromechanisms are responsible for determining the fracture toughness of all ten high purity 7075 aluminum alloys.

Fractographic analysis indicated a distinct difference in the number of large ductile dimples present with different levels of purity. In addition, smaller dimples are found between the large iron and silicon particles in all the alloys. The chromium-bearing alloys had dimples on the order of 1.0 μm, while 0.25 to 0.50 μm dimples were present in the zirconium-bearing alloys. The size of these smaller dimples found between the iron and silicon particles appears to be related to the heat treatment.

Past research has shown that fracture toughness is increased by controlling the amount of constituent particles present. If fracture toughness is controlled by only the amount of iron and silicon present, then one must conclude that either failure is a one-step process, or the purity levels are not sufficiently high to insure that the second stage becomes active. The fractographic results of this work suggest that a second stage occurred; the plots of W/A *vs* purity suggest that the second stage becomes significant at 0.2 wt pct Fe + Si.

It appears that iron and silicon levels of 0.11 are the lowest values considered to be commercially feasible.[24] This purity level is sufficiently high to have a two-step failure process where the finer particles control the second stage. The distribution, size, and type of these finer particles are determined during the final thermomechanical processing. This suggests judicious choice of thermomechanical processing can improve fracture toughness at equivalent strength levels. Recent work on high strength powder aluminum forgings[25] where there are no "macroinclusions" shows an increase from 26.1 to 35.0 KSI-in.$^{1/2}$ (28.7 to 38.5 MPa-m$^{1/2}$) in the short transverse toughness at a yield strength of 71.1 KSI (490.6 MPa). This difference in toughness is due to different hot-working and heat-treating sequences. Perhaps the most convincing argument that high purity is a necessary but not a sufficient condition for good fracture toughness is the alloy 7475 itself. The greater toughness of 7475 (*vs* that of 7075) is attributed to both the proprietary processing (Alcoa 467 Process) and its cleaner structure.[26]

ACKNOWLEDGMENTS

The author is indebted to Mr. C. O. Smith, Mr. R. Pence and Mr. R. Omlor for their assistance in the testing phase of the program. Advice on the use and interpretation of an analysis of variance by Mr. J. F. Santner is acknowledged. Discussions with Dr. T. M. F. Ronald, AFML, are also appreciated.

REFERENCES

1. *Influence of Iron and Silicon Content on the Tensile Properties of 7X75 and Zr-Modified 7X75 Aluminum Plate,* Technical Report Number AFML-TR-75-140, July 1975, Air Force Materials Laboratory, WPAFB, OH. (Available through NTIS, Department of Commerce, Springfield, Va. 22151.)
2. *Effect of Iron and Silicon Content on Stress Corrosion Cracking in a Thermomechanically Processed Aluminum Alloy,* Technical Report Number AFML-TR-75-43, July 1975, Air Force Materials Laboratory, WAPFB, OH. (Available through NTIS, Department of Commerce, Springfield, Va. 22151.)
3. *Effect of Iron and Silicon Content on the Fracture Toughness of 7X75 and Zr-Modified 7X75 Aluminum Plate,* Technical Report Number AFML-TM-LL-75-10, July 1975, Air Force Materials Laboratory, WPAFB, OH. (Available through NTIS, Department of Commerce, Springfield, Va. 22151.)
4. *High Strength Aluminum Alloy Development,* Technical Report Number AFML-TR-70-171, August 1970, Air Force Materials Laboratory, WPAFB, OH. (Available through NTIS, Department of Commerce, Springfield, Va. 22151.)
5. M. V. Hyatt and W. E. Quist: unpublished Boeing data 1967.
6. A. S. Tetelman and A. J. McEvily, Jr.: *Fracture of Structural Materials,* New York, John Wiley and Sons, Inc., 1967.
7. *Program to Improve the Fracture Toughness and Fatigue Resistance of Aluminum Sheet and Plate for Airframe Applications,* Technical Report Number AFML-TR-73-224, September 1973, Air Force Materials Laboratory, WPAFB, OH 45433. (Available through NTIS, Department of Commerce, Springfield, Va. 22151.)
8. J. Waldman, H. Sulinski, and H. Markus: *Met. Trans.,* 1974, vol. 5, pp. 573-84.
9. P. J. Blau: *Metallogr.,* 1975, vol. 7, pp. 187-201.
10. 1975 Annual Book of ASTM Standards, Part 10: *Metals-Mechanical, Fracture, and Corrosion Testing; Fatigue; Erosion; Effect of Temperature.* Proposed Method for Sharp-Notch Tension Testing of Thick High-Strength Aluminum and Magnesium Alloy Products with Cylindrical Specimens, pp. 799-810.
11. J. S. Santner and A. Gunderson: *Development of a Low Cost Reliable Test to Verify Fracture Toughness of Light Metal Alloys,* Mini-Symposium of New Avenues for Progress in Aerospace Research Technology & Systems, WPAFB, OH, 25 March 1976.
12. *Rapid Inexpensive Tests for Determining Fracture Toughness,* Report of the Committee on Rapid Inexpensive Tests for Determining Fracture Toughness, National Materials Advisory Board, Publication NMAB-328, National Academy of Science, Washington, D.C., 1976, (Available from Printing and Publishing Office, National Academy of Sciences, 2101 Constitution Avenue, N.W., Washington, D.C. 20418.)
13. A. W. Thompson and P. F. Weihrauch: *Scripta Met.,* 1976, vol. 10, pp. 205-10.
14. T. M. F. Ronald, J. A. Hall, and C. M. Pierce: *Met. Trans.,* 1972, vol. 3, pp. 813-18.
15. *Research on Synthesis of High-Strength Aluminum Alloys,* Technical Report Number AFML-TR-72-199, Part II, July 1973, Air Force Materials Laboratory, WPAFB, OH, (Available through NTIS, Department of Commerce, Springfield, Va. 22151.)
16. G. T. Hahn and A. R. Rosenfield: *Met. Trans. A,* 1975, vol. 6A, pp. 653-70.
17. G. T. Hahn and A. R. Rosenfield: *Relations Between Microstructure and the Fracture Toughness of Metals,* Third International Conference on Fracture, Paper PL-III-211, Munich, 1973.
18. D. Broek: *A Study on Ductile Fracture,* National Aerospace Laboratory, NRL, The Netherlands, NLR-TR-71021U, 1971.
19. R. H. Van Stone and J. A. Psioda: *Met. Trans. A,* 1975, vol. 6A, pp. 668-70.
20. J. S. Santner and M. E. Fine: *Met. Trans. A,* 1976, vol. 7A, pp. 601-04.
21. *Damage Tolerant Design Handbook,* Part I, January 1975, distributed by the National Technical Information Services, U.S. Department of Commerce, Springfield, Va. 22151.
22. E. DiRusso, M. Conserva, F. Gatto, and H. Markus: *Met. Trans.,* 1973, vol. 4, pp. 1133-44.
23. W. H. Reimann and A. W. Brisbane: *Eng. Fract. Mech.,* 1973, vol. 5, pp. 67-78.
24. *Improvement of Helicopter Forgings by Controlled Solidification and Thermal-Mechanical Treatments,* U.S. Army Aviation Systems Command, AVSCOM Report No. 76-41, October 1976, St. Louis, Mo. 63166. (Available through NTIS, U.S. Department of Commerce, Springfield, VA 22151.)
25. *Metallurgical Factors Controlling Structure in High Strength Aluminum P/M Products,* Technical Report Number AFML-TR-76-60, May 1976, Air Force Materials Laboratory, WPAFB, OH 45433. (Available through NTIS, U.S. Department of Commerce, Springfield, Va. 22151.)
26. J. M. Van Orden and D. E. Pettit: *Metal Progr.,* 1977, vol. 112, no. 8, pp. 28-31.